Anomalous Transport Signatures in Weyl Semimetals with Point Defects

J. P. Santos Pires,[1,2,*] S. M. João,[1,2,‡] Aires Ferreira,[3] B. Amorim,[4] and J. M. Viana Parente Lopes[1,2,†]
[1]Departamento de Física e Astronomia, Faculdade de Ciências da Universidade do Porto, Rua do Campo Alegre, s/n, 4169-007 Porto, Portugal
[2]Centro de Física das Universidades do Minho e do Porto (CF-UM-UP) and Laboratório de Física para Materiais e Tecnologias Emergentes LaPMET, University of Porto, 4169-007 Porto, Portugal
[3]Department of Physics and York Centre for Quantum Technologies, University of York, YO10 5DD York, United Kingdom
[4]Centro de Física das Universidades do Minho e do Porto (CF-UM-UP) and Laboratório de Física para Materiais e Tecnologias Emergentes LaPMET, Universidade do Minho, Campus de Gualtar 4710-057 Braga, Portugal

(Received 31 May 2022; accepted 12 October 2022; published 3 November 2022)

We present the first theoretical study of transport properties of Weyl semimetals with point defects. Focusing on a class of time-reversal symmetric Weyl lattice models, we show that dilute lattice vacancies induce a finite density of quasilocalized states at and near the nodal energy, causing strong modifications to the low-energy spectrum. This generates novel transport effects, namely, (i) an oscillatory behavior of the dc conductivity with the charge carrier density in the absence of magnetic fields, and (ii) a plateau-shaped dissipative optical response for photon frequencies below the interband threshold, $E_F \lesssim \hbar\omega \lesssim 2E_F$. Our results provide a path to engineer unconventional quantum transport effects in Weyl semimetals by means of common point defects.

DOI: 10.1103/PhysRevLett.129.196601

Weyl semimetals (WSMs) are a new class of topological materials whose low-energy excitations behave as chiral Weyl fermions in $(3+1)$ dimensions [1]. Their nontrivial topology, resulting from the separation of Weyl nodes with opposite chirality in momentum space, finds one of its prime manifestations in unusual surface states called Fermi arcs [2–6]. Because WSMs provide a route towards the realization of the chiral anomaly, they have become a bedrock for the correspondence between quantum field theory and condensed matter physics [7–12].

WSMs likewise provide a fertile ground for exploring the interplay of band topology and disorder effects, both from the perspective of quantum phase transitions at zero temperature [13–16] and key transport signatures of the chiral anomaly, such as the chiral magnetic effect [17–19]. Moreover, theoretical studies indicate that the topological protection enjoyed by clean WSMs survives the inclusion of smooth disordered potentials, rendering well-decoupled Weyl nodes [20–22] connected by robust surface Fermi arcs [23–25].

Meanwhile, the impact of realistic disorder landscapes beyond the standard mean-field picture has proved to be a subtle and intriguing problem [26,27]. The inevitable existence of so-called *rare regions* within a disorder landscape, in which the scattering potential attains a constant value, was found to yield a small, *but nonzero*, density of states (DOS) at the nodal energy [28–32]. Rare fluctuations of the disorder potential induce power-law localized resonances within the continuum [28] (not unlike the Lifshitz-tail phenomenon [33,34]), which are manifest in weakly disordered samples with arbitrarily long elastic scattering lifetimes and statistically relevant in the thermodynamic limit [32]. Notwithstanding, rare-region events produce a minute effect on measurable quantities (the nodal DOS lifting is exponentially small in the inverse disorder strength [28,29]), which makes them very challenging to detect. With this in mind, this Letter discusses alternative mechanisms that can yield *distinctive model-free signatures of resonant zero-energy states amenable to experimental verification*. We posit that vacancies are ideal candidates for this purpose because they are common point defects that act as strong scatterers of charge carriers, also preserving the nonspatial symmetries of the underlying lattice model [35–38]. Moreover, vacancies can be intentionally created by light-ion irradiation [39,40] and have been shown to generate *scale-free bound states* at the nodal energy of WSMs [41], thus providing a practical route to explore transport signatures of emergent zero-energy modes under controlled conditions. Point defects are expected to be chiefly important in WSMs of the TaAs family, including NbAs, TaP, and NbP, which typically crystalize as cubic lattices. These can be synthesized by standard chemical vapor transport techniques [42] and are experimentally known to host a significant concentration of point defects, even in the highest quality crystals [43,44].

Here, we report new real-space simulations of charge carrier transport and optical response in a time-reversal symmetric WSM hosting a finite concentration of point defects. Our study reveals several novel transport effects. First, the electrical conductivity is shown to display an

oscillatory behavior on top of the standard monotonic variation with the charge carrier density. This is in stark contrast to the monotonic dependence in analogous 2D Dirac models [38], and cannot be easily replicated by other disorder species. Rather, it derives from strong intervacancy interference effects that efficiently modulate the response of the Fermi surface to external fields in slightly doped WSMs. Second, and equally important, the optical response of WSMs with dilute vacancy defects exhibits uniform absorption over a wide frequency range, $E_F \lesssim \hbar\omega \lesssim 2E_F$, below the onset of interband transitions. This effect is a unique manifestation of emergent nodal bound states amenable to experimental verification. Finally, additional numerical results on the electronic structure are also shown with the aim of deciphering vacancy-induced zero energy modes and characterizing their sensitivity to applied magnetic fields.

Electronic structure.—The WSM is described by a two-orbital tight-binding model defined on a simple cubic lattice ($\mathcal{L}$),

$$\mathcal{H}_0 = \frac{\hbar v}{2ia}\sum_{\mathbf{R}\in\mathcal{L}}\sum_{i=x,y,z}[\Psi^\dagger_{\mathbf{R}}\cdot\sigma^i\cdot\Psi_{\mathbf{R}+a\mathbf{x}_i} - \text{H.c.}], \quad (1)$$

where a is the lattice parameter, v is the Fermi velocity, $\mathbf{x}_j = (\hat{x},\hat{y},\hat{z})$ are the Cartesian unit vectors, $\boldsymbol{\sigma}$ is a vector of 2×2 Pauli matrices, and $\Psi^\dagger_{\mathbf{R}} = [c^\dagger_{\mathbf{R},1}, c^\dagger_{\mathbf{R},2}]$ is a local two-orbital fermionic creation operator [31]. A *full vacancy* acts as a local perturbation that removes all hoppings between orbitals at the defect site and its neighbors. In a companion paper [41], we have shown that one such point defect produces a bound state at the nodal energy whose real-space wave function decays asymptotically with an inverse-square law. In what follows, we employ large-scale Chebyshev expansions of lattice Green's functions [38,45], as implemented in the KITE code [46], to determine the impact of vacancy-induced nodal states on several quantities of interest.

We start by calculating the change to the thermodynamic DOS induced by a finite concentration of randomly placed vacancies, n_v. We recall that the clean DOS vanishes quadratically at the nodal energy and hence a pristine WSM realizes an incompressible electronic phase in the absence of external fields. Unsurprisingly, symmetry breaking due to disorder will change this picture by transferring spectral weight across the energy spectrum, with previous studies of white-noise scalar potentials and extended impurities showing that the significant changes in the DOS occur away from the nodal energy, owing to the topological protection enjoyed by Weyl fermions [28–32]. Moreover, the situation with vacancies is strikingly different. If random vacancies within a sample were taken in isolation, the single-vacancy result of Ref. [41] would imply that a spectral weight proportional to n_v would be drawn out of the continuum and placed exactly at the nodal energy. Generally speaking, such a situation cannot

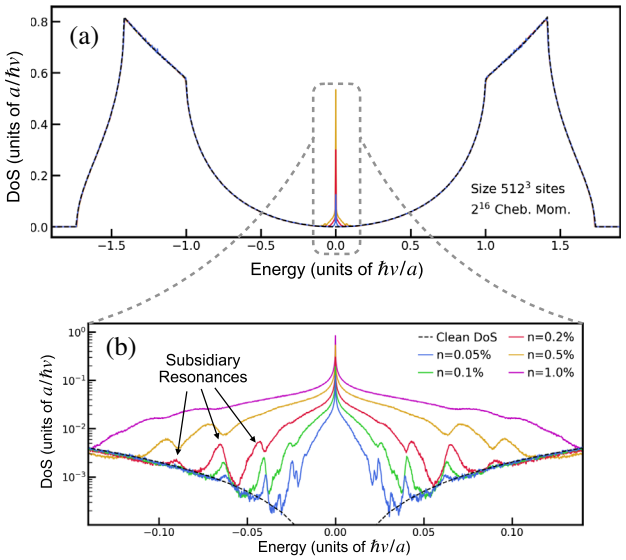

FIG. 1. Average DOS of a large WSM lattice, with linear size $L = 512a$, for several vacancy concentrations. An overview of the entire spectrum is presented in (a) and a close-up around the central peak is shown in (b). The comb of subsidiary resonances is marked by arrows in (b). The spectral resolution of the calculations was set to $10^{-3}\hbar v/a$.

be maintained for sufficiently large defect concentrations and, in fact, coherent multiple-scattering may become important in the quantum regime, even at low concentrations [38,47].

To reliably capture quantum coherence effects, we consider large cubic systems with linear size L. The DOS is obtained by simulating a system with $L = 512a$ using an exact Chebyshev expansion of the resolvent operator convoluted with a Jackson damping kernel [45]. Finite size effects are eliminated by jointly averaging over defect configurations and random twisted boundary conditions, which yield virtually exact simulations within resolution. Our results, summarized in Fig. 1, disclose a strong enhancement in and around the node for any nonzero vacancy concentration. As anticipated, this sharply contrasts with the case of a random on-site potential disorder where the nodal DOS change is exponentially small in the inverse of the perturbation parameter. Furthermore, as n_v is increased, a wider symmetrical structure emerges at the base of the central peak, signaling that intervacancy hybridization is turning the bound states into continuum resonances and spreading their weight over a finite spectral region. Interestingly, this energy spreading entails a finer structure of subsidiary peaks that flank the node for dilute concentrations, $n_v \lesssim 1\%$; see Fig. 1(b). This comb of sharp resonances is characteristic of three-dimensional (3D) WSMs and cannot be observed in the DOS of a 2D Dirac semimetal with vacancies [41].

Magnetic response.—We have argued that, in general, quantum interference effects between vacancies lift the degeneracy of zero-energy modes, thus generating sharp resonances shifted away from the node. These hybrid states

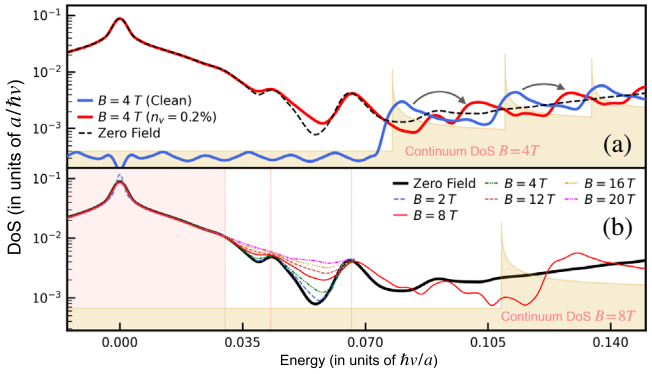

FIG. 2. (a) DOS of a system with (red) and without (blue) dilute vacancies subjected to a 4 T magnetic field along $\mathbf{z}$. (b) DOS with a vacancy concentration of $n_v = 0.2\%$ for a selection of magnetic field strengths. Insensitive regions of the spectrum are marked or shaded in salmon. Above $E = 0.07\hbar v/a$, only the curves for $B = 0$ and 8 T are represented. In both cases, the zero field curves are shown in black and the low-energy theory DOS appear in the background, a lattice spacing of $a = 5$ Å was assumed, and the spectral resolution was set to $10^{-3}\hbar v/a$.

are no longer proper bound states but, crucially, still retain a quasilocalized character. In Ref. [41] this picture was confirmed by exact diagonalization results, while here we take a less direct but more practical approach. Rather than probing the real-space wave functions, we scrutinize the modification to the DOS induced by an external uniform magnetic field in the presence of vacancies. The rationale for this is that quasilocalized electronic states should remain robust to applied magnetic fields, thus effectively freezing out the DOS around the nodal energy. This intuition is backed by our DOS simulations for selected field strengths in the range 2 to 20 T shown in Fig. 2. We also present the DOS calculated in the clean system for a direct comparison at a finite B. Two features are worth mentioning. First of all, near the nodal energy, the DOS stays pinned to its zero-field values which corroborates the quasilocalized character of defect states. Indeed, the DOS central peak [shaded region in Fig. 2(b)] and the subsidiary resonances (vertical dashed lines) are nearly unchanged by the external field. This contrasts with the regions in between the subsidiary resonances, as shown in Fig. 2(b), and also with the characteristic plateau-shaped DOS expected in a clean Weyl node, whose $n = 0$ (chiral) Landau level disperses linearly along the magnetic field [48–50]. Second, the set of DOS peaks (van Hove singularities) at the bottom of the nonchiral Landau levels is largely unaffected by the addition of point defects, except for the global shift away from the nodal energy as indicated by the arrows in Fig. 2(a). This reinforces the notion that vacancies introduce new (quasilocalized) states around zero energy, but trivially affect the electronic structure far from it.

Bulk transport and diffusivity.—The DOS of a bulk 3D system is not easily accessible to experiments, but it directly influences a range of thermodynamic and transport properties. An experimentally measurable quantity of great interest is the bulk dc conductivity. In the diffusive regime, the latter is related to the DOS at the Fermi level according to $\sigma_{\rm dc}(E_F) = e^2\rho(E_F)\mathcal{D}(E_F)$, where $\mathcal{D}(E_F)$ is the electronic diffusivity. Thereby, the strong energy dependence imparted by vacancies on the DOS (i.e., the emergent nodal peak and the comb of subsidiary resonances; see Fig. 1) is expected to have a counterpart on the electrical conductivity. To explore this further, we evaluate the $T = 0$ linear dc conductivity of systems with a finite vacancy concentration using the Kubo-Greenwood formula [51,52]

$$\sigma^{ii}_{\rm dc}(E_F) = \left\langle \frac{e^2h}{a^3L^3}\mathrm{Tr}[\mathscr{V}^i\delta_\eta(E_F-\mathcal{H}_v)\mathscr{V}^i\delta_\eta(E_F-\mathcal{H}_v)]\right\rangle, \tag{2}$$

where $\mathcal{H}_v$ is the Hamiltonian with random point defects, $\mathscr{V}^i = (i/\hbar)[\mathcal{H}_v, \hat{x}_i]$ is the velocity operator along $\hat{x}_i$ [53], Tr is the trace operation, and $\langle\cdots\rangle$ represents the configurational average over the vacancy distribution. The numerical evaluation of Eq. (2) is carried out with the efficient single-shot Chebyshev polynomial Green's function method [38,46], and requires a broadening of the Dirac-δ functions by a spectral resolution $\eta \gtrsim \delta\varepsilon$, where $\delta\varepsilon$ is the mean-level spacing. We note that the broadening parameter can alternatively be viewed as playing the role of aphenomenological self-energy with origin in electron-phonon scattering events [54]. Because we are interested in disorder-limited charge carrier transport, hereafter we focus on the behavior of $\sigma_{\rm dc}$ in the thermodynamic limit with $\eta \to \delta\varepsilon$. In Fig. 3, we present the fully converged results of our Kubo simulations with spectral resolutions down to $\eta = 5\times10^{-4}\ \hbar v/a$. Strikingly, these results show that the WSM dc conductivity is strongly nonmonotonic at low energies, which makes point defects strong contenders for studies of quantum interference effects by means of standard electrical transport measurements at zero magnetic fields. Indeed, the Fermi level dependence of

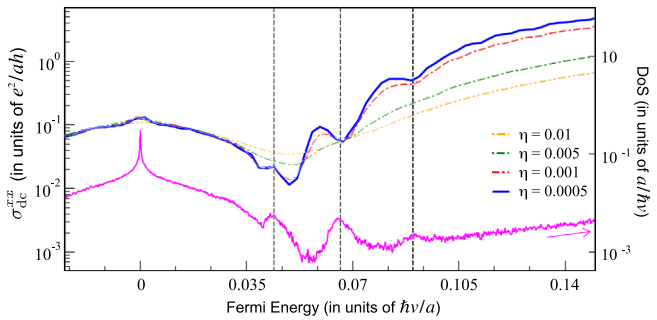

FIG. 3. Zero temperature bulk dc conductivity as a function of the Fermi energy for several values of the inelastic broadening, η. The DOS is also depicted in magenta for reference, with the vertical black lines indicating prominent subsidiary resonances. The vacancy concentration was fixed to $n_v = 0.2\%$.

$\sigma_{\mathrm{dc}}^{xx}$ is seen to nicely track the oscillatory behavior of the DOS (see Fig. 3), confirming the intuition that the novel spectral fingerprints of point defects are reflected on the linear-response properties. We expect this oscillatory behavior in the dc conductivity to remain visible up to moderate temperatures (on the order of 100 K) as long as the oscillation scale ($\sim 0.01\ \hbar v/a$) remains sizable compared to the thermal broadening (see Supplemental Material [55] for additional discussions). Additionally, our quantum transport simulations reveal that the spectral convergence rate (which measures how quickly the conductivity curves saturate with decreasing η) is strongly dependent on the precise Fermi level location in the low energy regime. We attribute this effect to a strong energy dependence of the disorder self-energy and related elastic scattering times [47]. Indeed, the dips observed at the resonant energies signal a *strong suppression of electron diffusivity*. This is a signature of scattering cross sections that are enhanced at these energies [56] by coherent multiple scattering processes among a few vacancies (see also Ref. [41]).

Optical response.—Next, we search for the optical signatures of the novel effects described above. Naively, the existence of a macroscopic number of zero energy modes generated by vacancy defects is expected to significantly change the allowed single-photon optical transitions. For a pristine, but slightly doped WSM, vertical interband transitions are Pauli blocked for $\omega < 2|E_F|$. This defines the system's optical gap, where the optical conductivity is mostly imaginary and reverses sign at $\omega = |E_F|$. In Fig. 4(a), the optical response of the clean WSM is represented in blue, where a linear growth of the conductivity's real part with ω can be seen above the optical gap [57]. This frequency dependence is a hallmark of 3D systems with linear dispersion, differing from the universal plateau-shaped infrared conductivity of graphene [58].

To account for the impact of randomly distributed vacancies, we have calculated the linear optical conductivity by means of a kernel-convoluted Chebyshev expansion of the finite-frequency Kubo formula [46,59,60]. Our findings are summarized in Fig. 4. In stark contrast to the standard situation without point defects, *a finite dissipative response now appears as a conductivity plateau in the interval* $|E_F| < \omega < 2|E_F|$.We note that the plateauheight grows quickly with the vacancy concentration n_v, and thus should be observable under realistic experimental conditions. For completeness and contrast, we also show the optical conductivity of the WMS lattice model with a box distribution of on-site disorder (of strength W) and no point defects; see Figs. 4(a)–4(b). In this case, the uncorrelated random potential produces a conventional broadening of the optical gap transition without specific features.

To explain the unusual optical response reported here, we note that vacancies act as resonant defects that introduce a macroscopic number of states near the band center of a time-reversal symmetric ($\mathcal{T}$-symmetric) Weyl lattice, and

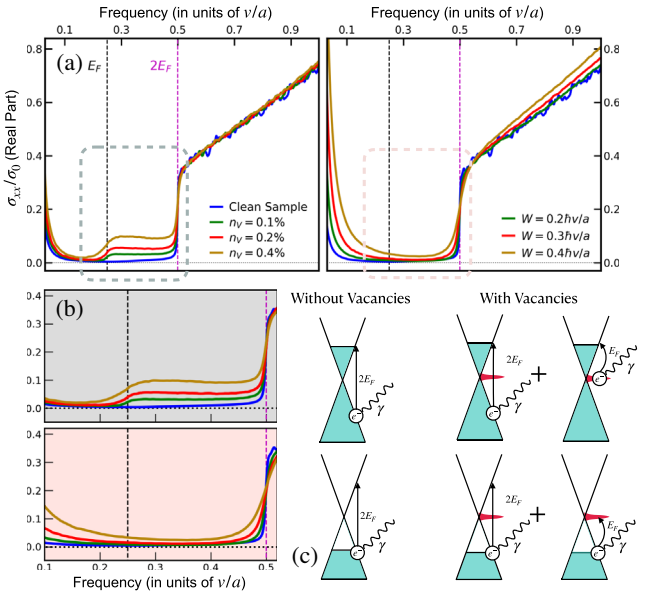

FIG. 4. (a) Longitudinal linear optical conductivity of a doped WSM computed with an energy broadening $\eta = 0.004\hbar v/a$ and a Fermi energy $\varepsilon_F = 0.25\hbar v/a$ with a finite vacancy concentration. The clean case is shown in blue. (b) Close-up of the vacancy-induced features in $\sigma_{xx}(\omega)$. (c) Relevant physical mechanisms for $\omega > |E_F|$. Vertical arrows represent interband transitions between Bloch states, while curved arrows indicate transitions between Bloch states and nodal quasibound states. All plots are converged in the number of polynomials.

that such states strongly break translation symmetry owing to their quasilocalized character. Hence, the vacancy defects efficiently participate in momentum nonconserving (but energy conserving) transitions involving extended states at the Fermi energy; see schematic in Fig. 4(c). These processes give a strong contribution to the real part of the conductivity starting at $\omega = |E_F|$, thus providing an unambiguous signature of defect-induced nodal modes accessible to experiments. Interestingly, the sharpness of transition to the vacancy-induced absorption regime at $\omega = \varepsilon_F$ provides an estimate to the width of the central peak in the DOS, and thus the extent of quantum-coherent intervacancy hybridization.

Conclusions and outlook.—Hitherto unknown effects of vacancies in the electronic structure, charge carrier transport, and optical response of a cubic $\mathcal{T}$-symmetric Weyl semimetal were investigated using real-space Green's function calculations. The first new insight is the emergence of a strong enhancement of the DOS in and around the nodal energy (see Ref. [41] for a complementary study of vacancy-induced bound states), which is in contrast to the previously studied cases of nonresonant disorder. As the defect concentration is increased, an efficient buildup of intervacancy hybridization effects leads to a broadening of the nodal DOS peak and, different from the established picture for 2D Dirac semimetals, also gives rise to a symmetric comb of subsidiary resonances at finite energies.

The vacancy-induced states are quasilocalized in real space, remain largely insensitive to applied magnetic fields and possess low quantum diffusivity. In addition, these features are also robust to further perturbations [41] which hints that they will likely be present in real WSM crystals, going beyond the model analyzed here.

Our main focus was on exploring experimentally accessible routes to observe distinctive signatures of resonant scattering by point defects in cubic Weyl semimetals, a relevant source of disorder even in high-quality single crystals such as those belonging to the cubic or tetragonal TaAs family [43,44]. Two major transport effects amenable to experimental detection were predicted. First, we showed that the Fermi-energy dependence of the low-temperature dc conductivity is characterized by an unusual oscillatory behavior showing a series of dips whenever a subsidiary resonance crosses the Fermi level. There, the effect of an enhanced DOS is compensated by the strongly suppressed electron diffusivity due to the quasilocalized nature of the states. We anticipate that such a strong Fermi level dependence would be amplified in measurements of the thermoelectric power, which is proportional to $d\sigma(E_F)/dE_F$ by Mott's formula [61]. Finally, we showed that vacancy-induced states endow the Weyl system with a unique optical response, i.e., the emergence of a plateau-shaped linear absorption below the interband threshold. Since it does not qualitatively depend on the Fermi level, this optical route is particularly appealing for studying bulk samples where the carrier density is notoriously difficult to control [62,63]. Our findings spotlight the role of point defects in amplifying quantum interference fingerprints in transport phenomena, setting the stage for understanding the interplay of topology and resonant disorder in generic Weyl semimetals.

J. P. S. P., S. M. J., B. A., and J. M. V. P. L. acknowledge support from the Portuguese Foundation for Science and Technology (FCT) within the Strategic Funding UIDB/04650/2020, and through projects No. POCI-01-0145-FEDER-028887 (J. P. S. P., S. M. J., and J. M. V. P. L.) and No. CEECIND/02936/2017 (B. A.). J. P. S. P. and S. M. J are funded by FCT Grants No. PD/BD/142774/2018 and No. PD/BD/142798/2018, respectively. A. F. acknowledges support from the Royal Society (London) through a Royal Society University Research Fellowship. The large-scale calculations were undertaken on the HPC Viking Cluster of the University of York. We thank J. Dieplinger, J. M. B Lopes dos Santos, and A. Altland for fruitful discussions, and David T. S. Perkins for proofreading the manuscript. We also thank the anonymous referees for providing valuable feedback.

*up201201453@fc.up.pt
†jlopes@fc.up.pt
‡Present address: Department of Materials, Imperial College London, South Kensington Campus, London SW7 2AZ, United Kingdom.

[1] N. P. Armitage, E. J. Mele, and A. Vishwanath, Rev. Mod. Phys. **90**, 015001 (2018).
[2] X. Wan, A. M. Turner, A. Vishwanath, and S. Y. Savrasov, Phys. Rev. B **83**, 205101 (2011).
[3] E. Witten, Riv. Nuovo Cimento **39**, 313 (2016).
[4] F. D. M. Haldane, arXiv:1401.0529.
[5] K. Hashimoto, T. Kimura, and X. Wu, Prog. Theor. Exp. Phys. **2017**, 053I01 (2017).
[6] B. Q. Lv, T. Qian, and H. Ding, Rev. Mod. Phys. **93**, 025002 (2021).
[7] A. A. Zyuzin and A. A. Burkov, Phys. Rev. B **86**, 115133 (2012).
[8] P. Hosur, Phys. Rev. B **86**, 195102 (2012).
[9] D. T. Son and B. Z. Spivak, Phys. Rev. B **88**, 104412 (2013).
[10] C.-L. Zhang *et al.*, Nat. Commun. **7**, 10735 (2016).
[11] E. Barnes, J. J. Heremans, and D. Minic, Phys. Rev. Lett. **117**, 217204 (2016).
[12] N. P. Ong and S. Liang, Nat. Rev. Phys. **3**, 394 (2021).
[13] K. Kobayashi, T. Ohtsuki, K.-I. Imura, and I. F. Herbut, Phys. Rev. Lett. **112**, 016402 (2014).
[14] J. H. Pixley, P. Goswami, and S. Das Sarma, Phys. Rev. Lett. **115**, 076601 (2015).
[15] S. Bera, J. D. Sau, and B. Roy, Phys. Rev. B **93**, 201302(R) (2016).
[16] B. Roy, R.-J. Slager, and V. Juričić, Phys. Rev. X **8**, 031076 (2018).
[17] A. A. Burkov, Phys. Rev. Lett. **113**, 247203 (2014).
[18] H.-Z. Lu and S.-Q. Shen, Phys. Rev. B **92**, 035203 (2015).
[19] A. A. Burkov, Phys. Rev. B **96**, 041110(R) (2017).
[20] Y. Ominato and M. Koshino, Phys. Rev. B **89**, 054202 (2014).
[21] A. Altland and D. Bagrets, Phys. Rev. Lett. **114**, 257201 (2015).
[22] A. Altland and D. Bagrets, Phys. Rev. B **93**, 075113 (2016).
[23] C.-Z. Chen, J. Song, H. Jiang, Q.-f. Sun, Z. Wang, and X. C. Xie, Phys. Rev. Lett. **115**, 246603 (2015).
[24] S. Liu, T. Ohtsuki, and R. Shindou, Phys. Rev. Lett. **116**, 066401 (2016).
[25] E. Brillaux and A. A. Fedorenko, Phys. Rev. B **103**, L081405 (2021).
[26] J. H. Pixley, P. Goswami, and S. Das Sarma, Phys. Rev. B **93**, 085103 (2016).
[27] M. Buchhold, S. Diehl, and A. Altland, Phys. Rev. Lett. **121**, 215301 (2018).
[28] R. Nandkishore, D. A. Huse, and S. L. Sondhi, Phys. Rev. B **89**, 245110 (2014).
[29] J. H. Pixley, D. A. Huse, and S. Das Sarma, Phys. Rev. X **6**, 021042 (2016).
[30] J. H. Wilson, D. A. Huse, S. Das Sarma, and J. H. Pixley, Phys. Rev. B **102**, 100201(R) (2020).
[31] J. Pixley and J. H. Wilson, Ann. Phys. (Amsterdam) 435, 168455 (2021).
[32] J. P. Santos Pires, B. Amorim, A. Ferreira, İ. Adagideli, E. R. Mucciolo, and J. M. Viana Parente Lopes, Phys. Rev. Res. **3**, 013183 (2021).
[33] S. Yaida, Phys. Rev. B **93**, 075120 (2016).
[34] V. Gurarie, Phys. Rev. B **96**, 014205 (2017).

[35] V. M. Pereira, J. M. B. Lopes dos Santos, and A. H. Castro Neto, Phys. Rev. B **77**, 115109 (2008).
[36] P. M. Ostrovsky, I. V. Protopopov, E. J. König, I. V. Gornyi, A. D. Mirlin, and M. A. Skvortsov, Phys. Rev. Lett. **113**, 186803 (2014).
[37] V. Häfner, J. Schindler, N. Weik, T. Mayer, S. Balakrishnan, R. Narayanan, S. Bera, and F. Evers, Phys. Rev. Lett. **113**, 186802 (2014).
[38] A. Ferreira and E. R. Mucciolo, Phys. Rev. Lett. **115**, 106601 (2015).
[39] Z.-J. Zhang, Y.-L. Fu, W. Cheng, and F.-S. Zhang, Comput. Mater. Sci. **160**, 9 (2019).
[40] Y.-L. Fu, H.-B. Sang, W. Cheng, and F.-S. Zhang, Mater. Today Commun. **24**, 100939 (2020).
[41] J. P. Santos Pires, S. M. João, A. Ferreira, B. Amorim, and J. M. Viana Parente Lopes, companion paper Phys. Rev. B **106**, 184201 (2022).
[42] N. J. Ghimire, Y. Luo, M. Neupane, D. J. Williams, E. D. Bauer, and F. Ronning, J. Phys. Condens. Matter **27**, 152201 (2015).
[43] T. Besara, D. A. Rhodes, K.-W. Chen, S. Das, Q. R. Zhang, J. Sun, B. Zeng, Y. Xin, L. Balicas, R. E. Baumbach, E. Manousakis, D. J. Singh, and T. Siegrist, Phys. Rev. B **93**, 245152 (2016).
[44] H. W. Liu, P. Richard, L. X. Zhao, G.-F. Chen, and H. Ding, J. Phys. Condens. Matter **28**, 295401 (2016).
[45] A. Weiße, G. Wellein, A. Alvermann, and H. Fehske, Rev. Mod. Phys. **78**, 275 (2006).
[46] S. M. João, M. Anđelković, L. Covaci, T. G. Rappoport, J. M. Viana Parente Lopes, and A. Ferreira, R. Soc. Open Sci. **7**, 191809 (2020).
[47] S. M. João, J. M. Viana Parente Lopes, and A. Ferreira, J. Phys. Mater. **5**, 045002 (2022).
[48] H. Nielsen and M. Ninomiya, Phys. Lett. **130B**, 389 (1983).
[49] J. Shao and G. Yang, AIP Adv. **6**, 025312 (2016).
[50] J. Klier, I. V. Gornyi, and A. D. Mirlin, Phys. Rev. B **96**, 214209 (2017).
[51] R. Kubo, J. Phys. Soc. Jpn. **12**, 570 (1957).
[52] D. A. Greenwood, Proc. Phys. Soc. London **71**, 585 (1958).
[53] We will drop the *i* index, since the system has (on average) a cubic symmetry.
[54] D. J. Thouless and S. Kirkpatrick, J. Phys. C **14**, 235 (1981).
[55] See Supplemental Material at http://link.aps.org/supplemental/10.1103/PhysRevLett.129.196601 for additional results on the dc conductivity and optical response.
[56] B. Elattari and T. Kottos, Phys. Rev. B **62**, 9880 (2000).
[57] P. E. C. Ashby and J. P. Carbotte, Phys. Rev. B **89**, 245121 (2014).
[58] R. R. Nair, P. Blake, A. N. Grigorenko, K. S. Novoselov, T. J. Booth, T. Stauber, N. M. R. Peres, and A. K. Geim, Science **320**, 1308 (2008).
[59] T. P. Cysne, T. G. Rappoport, A. Ferreira, J. M. Viana Parente Lopes, and N. M. R. Peres, Phys. Rev. B **94**, 235405 (2016).
[60] S. M. João and J. M. Viana Parente Lopes, J. Phys. Condens. Matter **32**, 125901 (2020).
[61] N. F. Mott and E. A. Davis, *Electronic Processes in Non-Crystalline Materials*, 2nd ed., International series of monographs on physics (Clarendon Press, Oxford, 2012), pp. 52–56.
[62] J. E. Moore, Nat. Sci. Rev. **6**, 206 (2019).
[63] K. Halterman, M. Alidoust, and A. Zyuzin, Phys. Rev. B **98**, 085109 (2018).